

Supporting Information

Carboxylated Wood-based Sponges with Underoil Superhydrophilicity for Deep Dehydration of Crude Oil

Ming-Bang Wu^{a†}, Sheng Huang^{b†}, Chang Liu^a, Jian Wu^{b*}, Seema Agarwal^c, Andreas Greiner^{c*}, and Zhi-Kang Xu^{a,d*}

^aMOE Key Laboratory of Macromolecular Synthesis and Functionalization, and Key Laboratory of Adsorption and Separation Materials & Technologies of Zhejiang Province, Department of Polymer Science and Engineering, Zhejiang University, Hangzhou 310027, China

^bDepartment of Chemistry, Zhejiang University, Hangzhou 310027, China

^cMacromolecular Chemistry and Bavarian Polymer Institute, University of Bayreuth, Universitätsstrasse 30, Bayreuth 95440, Germany

^dCollege of Chemical and Biochemical Engineering, Zhejiang University, Hangzhou 310027, China

E-mails: jianwu@zju.edu.cn (J. Wu); greiner@uni-bayreuth.de (A. Greiner); xuzk@zju.edu.cn (Z.-K. Xu).

$$\gamma_{w/o} \cos \theta_{w/o} = \gamma_{w/a} \cos \theta_{w/a} - \gamma_{o/a} \cos \theta_{o/a} \quad (\text{Equation S1})$$

$$\gamma_{w/o} \cos \theta_{o/w} = \gamma_{o/a} \cos \theta_{o/a} - \gamma_{w/a} \cos \theta_{w/a} \quad (\text{Equation S2})$$

where the $\gamma_{w/o}$, $\gamma_{w/a}$, and $\gamma_{o/a}$ are the water/oil, water/air, and oil/air interface tension, respectively. The $\theta_{w/o}$, $\theta_{w/a}$, $\theta_{o/a}$ and $\theta_{o/w}$ are the underoil water contact angle, water contact angle in the air, oil contact angle in the air and underwater oil contact angle, respectively.

Then we add Equation S1 and Equation S2 to gain Equation S3 as follow:

$$\gamma_{w/o}(\cos \theta_{w/o} + \cos \theta_{o/w}) = 0 \quad (\text{Equation S3})$$

Finally, we can find only when $\theta_{w/o} + \theta_{o/w} = 180^\circ$ can always fit the Equation S3.

Table S1. Metal contents in the crude oil before and after treatment by CWS.

Type of metal	Metal contents before treatment (ppm)	Metal contents after treatment (ppm)
Al	87.415 ± 1.464	0.101± 0.004
Ca	72.957± 3.885	0.417± 0.121
V	11.046± 2.589	0.002± 0.001
Fe	328.943± 12.366	0.080± 0.035
Cu	58.265± 4.298	0.274± 0.421
Cd	3.0523± 0.124	0.121± 0.024

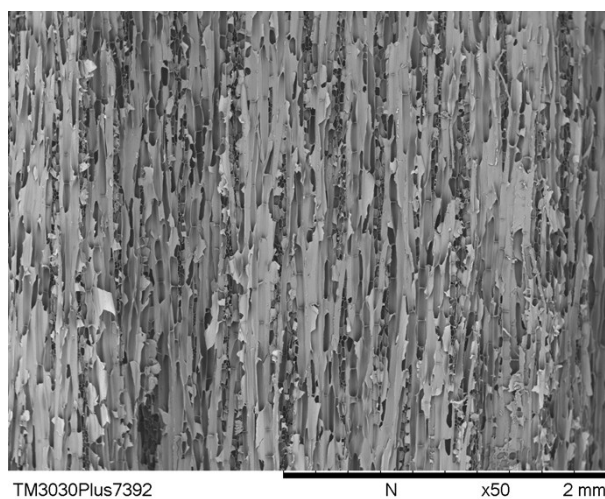


Figure S1. SEM image of the cross section from the a) natural balsa wood and b) wood-based sponge along the growing direction.

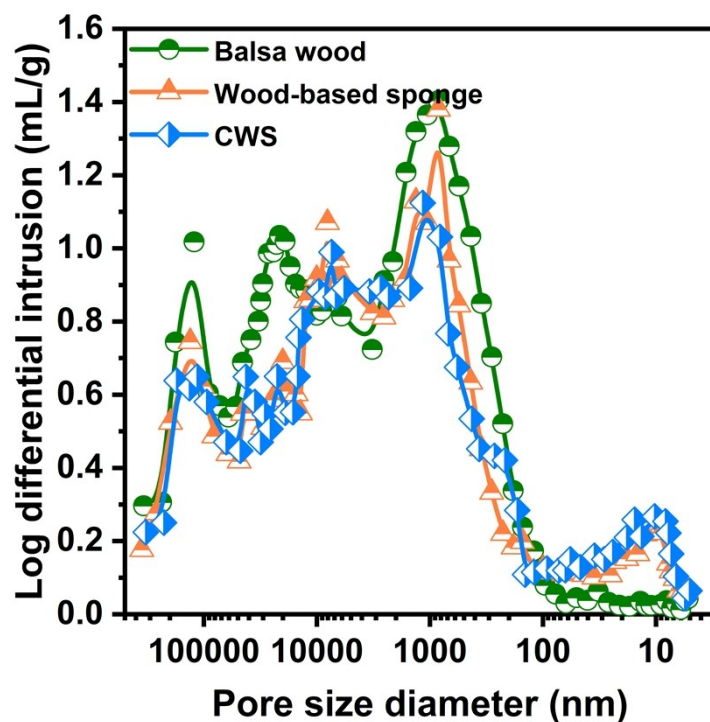


Figure S2. Pore size distribution of the natural balsa wood, wood-based sponge and the as-prepared CWS measured by mercury porosimeter.

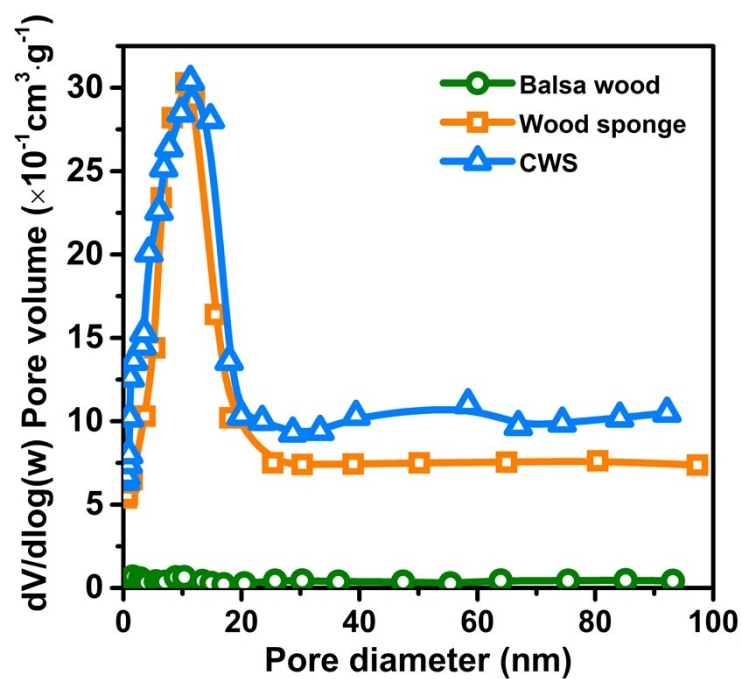


Figure S3. Pore size distribution of the natural balsa wood, the wood-based sponge and the as-prepared CWS obtained from BET method.

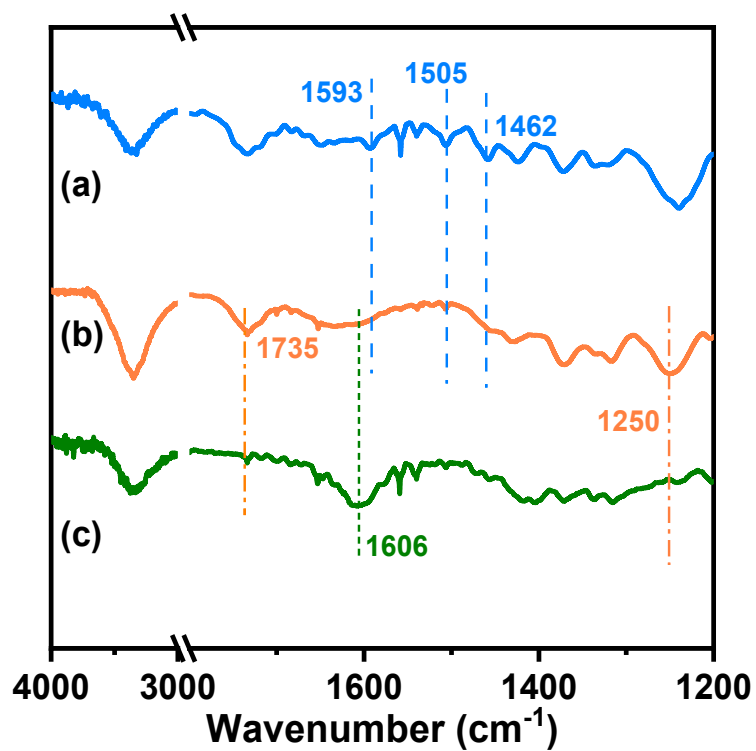


Figure S4. FT-IR spectra of the (a) natural balsa wood, (b) delignified wood, and (c) as-prepared CWS.

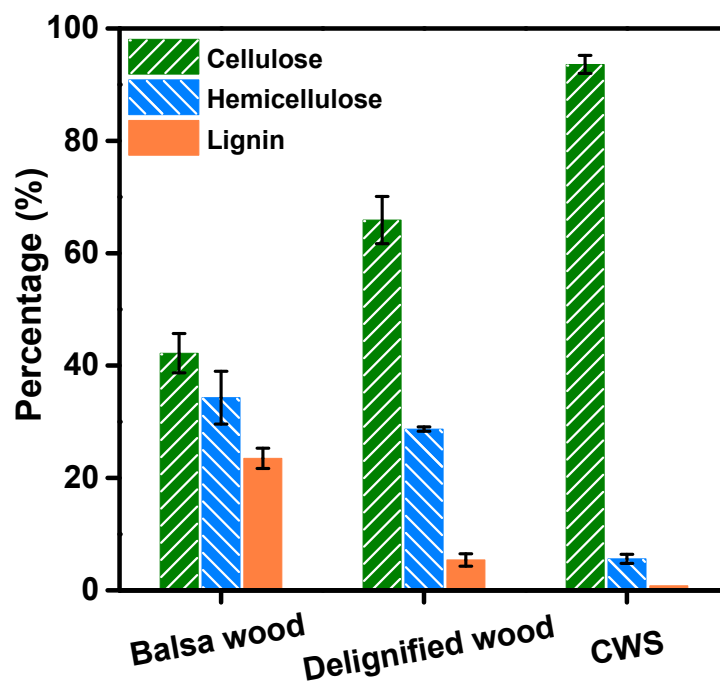


Figure S5. Chemical components of the natural balsa wood, the delignified wood, and the as-prepared CWS.

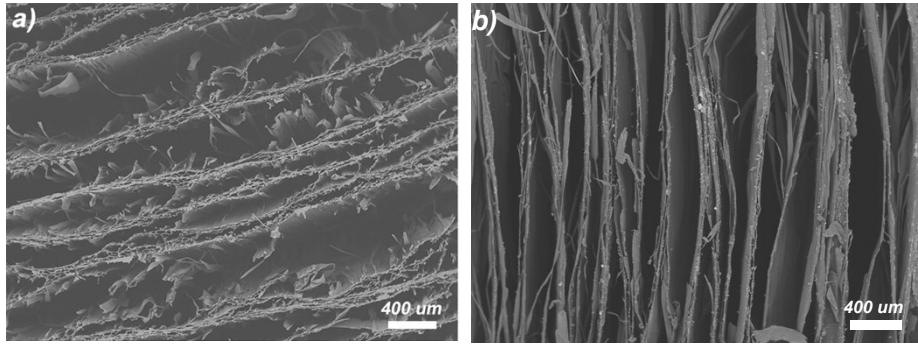


Figure S6. a) Surface SEM images of the wood-based sponge perpendicular to the growing direction. b) SEM images of the wood-based sponge along the growing direction.

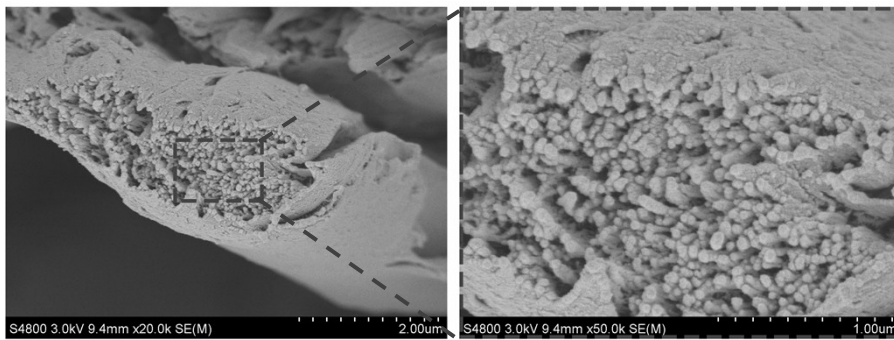


Figure S7. SEM images of the walls in wood-based sponges under high magnification.

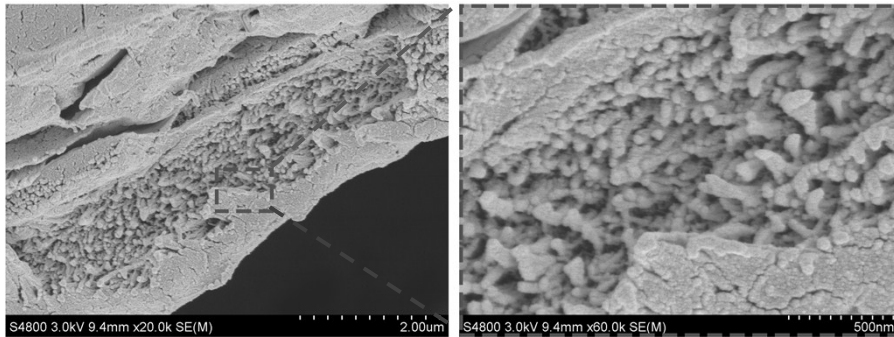


Figure S8. SEM images of the walls in CWS under high magnification.

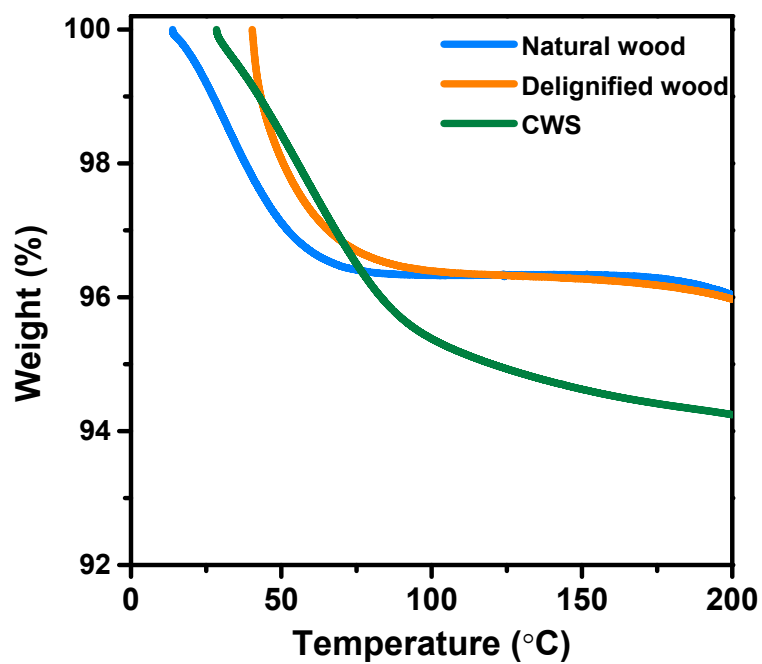


Figure S9. TGA analysis of the natural balsa wood, the delignified wood, and the as-prepared CWS.

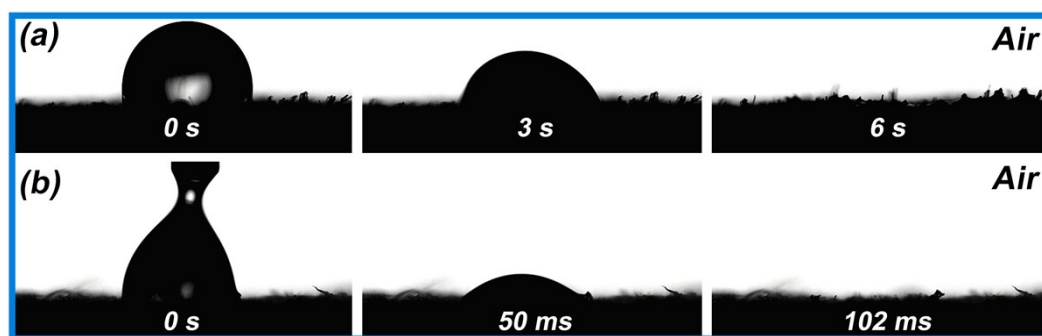


Figure S10. A series of photos taken when a water droplet is on the surfaces of a) balsa wood and b) CWS, respectively.

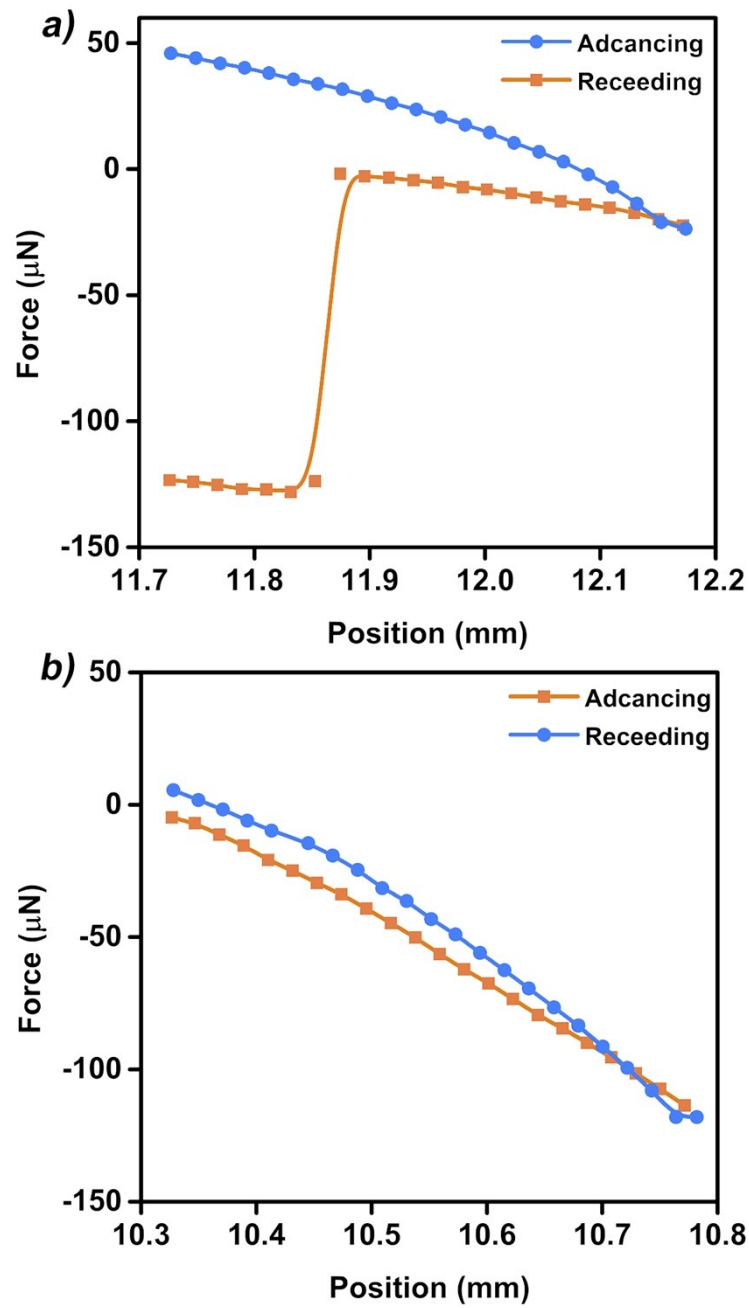


Figure S11. Force-distance curve of an underwater crude oil droplet on the surfaces of a) balsa wood and b) CWS, respectively.

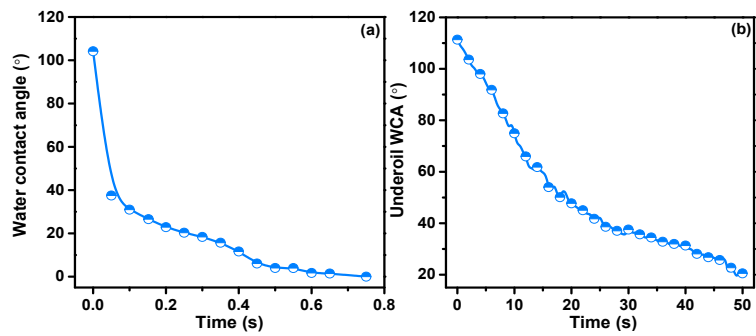


Figure S12. Wettability of CWS surfaces that along the growing direction. (a) Dynamic water contact angle in the air. (b) Dynamic underoil water contact angle.

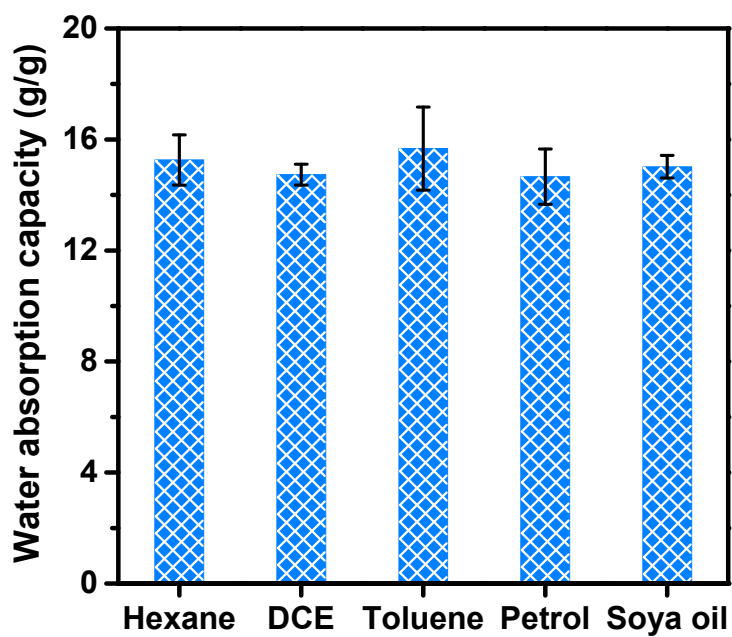


Figure S13. Water absorption capacity of the CWS from various oils and solvents.

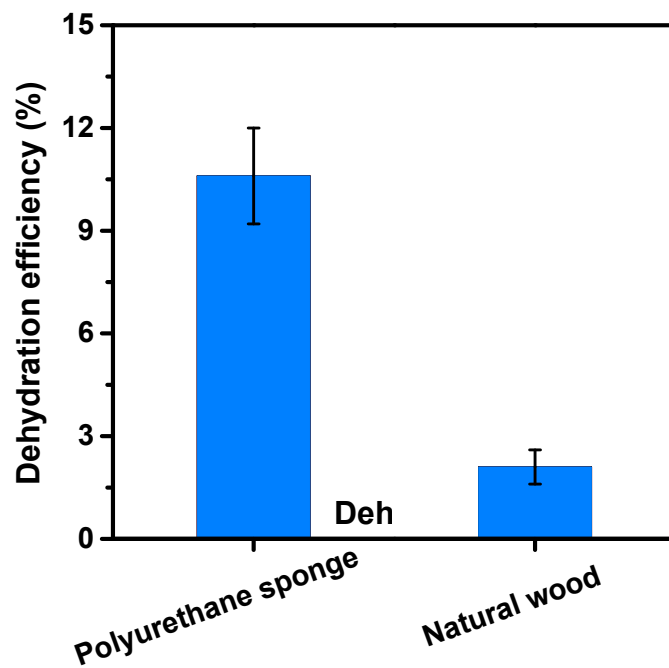


Figure S14. Dehydration efficiency of polyurethane sponge and natural wood when absorbing water from the water-in-crude oil emulsion.

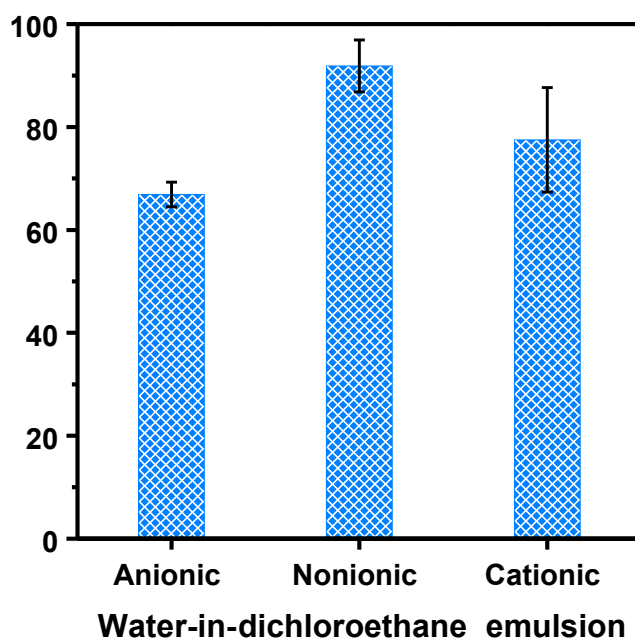


Figure S15. Dehydration efficiency of the CWS when absorbing water from the surfactant-stabilized water-in-dichloroethane emulsions.

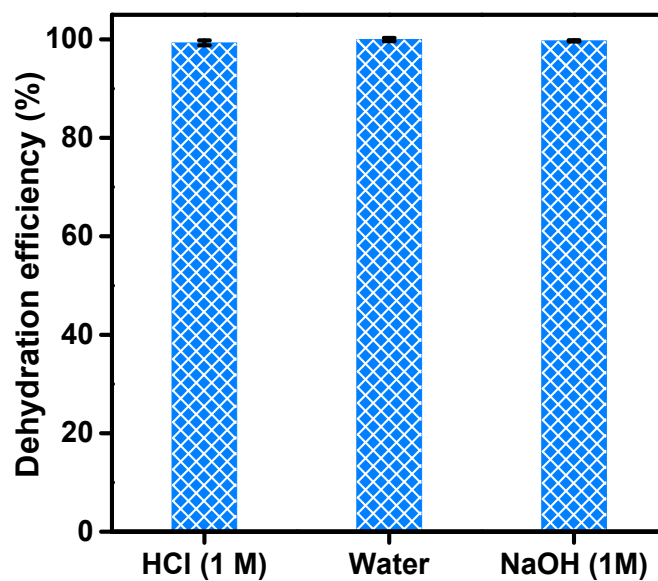


Figure S16. Dehydration efficiency of the CWS when absorbing water from the water-in-crude oil emulsion with different pH values.

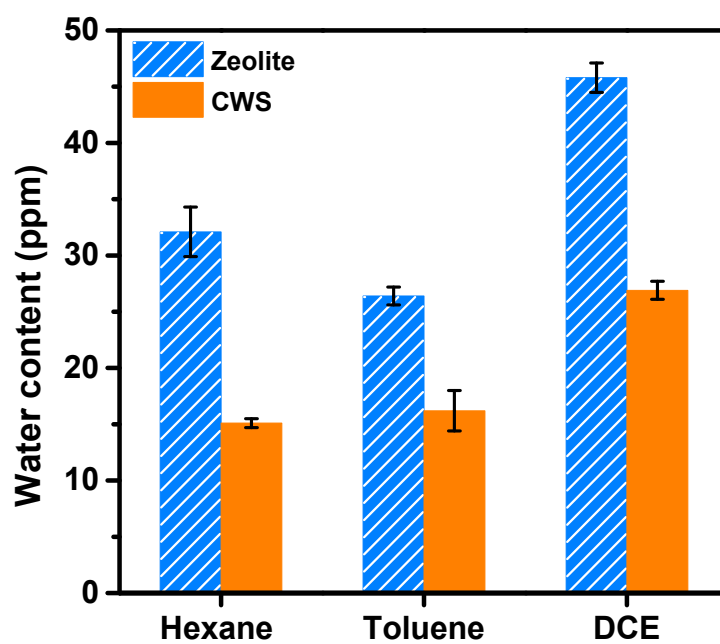


Figure S17. Water content in the water-immiscible solvents after dehydration with zeolite and CWS, respectively.

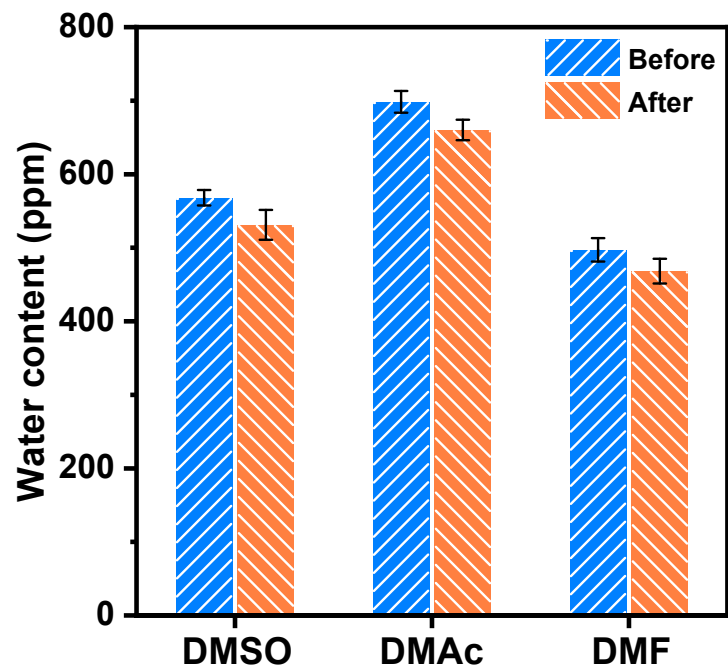


Figure S18. Water content in the water-soluble solvents including DMSO, DMAc and DMF before and after the dehydration treatment by CWS.